ISSN 1392 - 1207. MECHANIKA. 2011. 17(6): 630-636

Self-tuning of position feedback and velocity feedback of active vibration isolation system with 6 DOFs

F. H. Liao*, X. P. Li, Z. Y. Yuan*****
**Huazhong University of Science and Technology, 430074, Wuhan, China, E-mail:lfh159257@163.com*
***Huazhong University of Science and Technology, 430074, Wuhan, China, E-mail: xpli@public.wh.hb.cn*
****Shanghai Micro Electronics Equipment Co., Ltd , China, E-mail: yuanzy@smee.com.cn*

crossref http://dx.doi.org/10.5755/j01.mech.17.6.1006

1. Introduction

Vibration isolation systems are widely used in high-precision motion systems such as IC stepper and high-precision measurement devices such as electron microscope [1-3, 4]. Ground vibration and direct disturbance force such as motion stages lead to payload vibration. Traditionally, passive isolators, such as air springs and Euler springs, are employed to isolate the vibrations above 10 Hz [5]. However, the passive isolator amplifies the vibrations near the resonance frequency which is normally in range of 2 ~ 6 Hz and greatly degrades the performance of precision equipment.

Unlike passive isolator, Active Vibration Isolation System (AVIS) can isolate both base vibration and direct disturbance without amplifying vibrations near resonance frequency. For a typical 6-DOF AVIS, position loop and velocity loop are both employed to achieve high anti-vibration performance and maintain position stability [1, 6-8]. Instead of velocity feedbacks, force feedbacks or acceleration feedbacks are used in pneumatic vibration isolation system and in aerospace vibration isolation system [9-11], in order to realize sky-hook damping [12-13]. Generally, loop-shaping tuning method is used to determine parameters of the sky-hook damping loop and the position feedback loop in sequence. However, there are 12 feedback loops, and at least 18 parameters in a 6-DOF AVIS. So the loop-shaping tuning method costs much time and greatly depends on the operator's experience.

In this paper, a fast self-tuning procedure is presented to get optimal damping for the 6-DOF AVIS with sky-hook damping. Firstly, the dynamic model of the 6-DOF AVIS is built. Secondly, we propose the self-tuning procedure and simulate the performance. At last, the self-tuning controller is validated with an experiment.

2. Model of 6-DOF AVIS

2.1. Structure dynamics

A typical 6-DOF AVIS includes 3 vibration isolators, as shown in Fig. 1. The payload is supported by 3 vibration isolators displaced at the vertices of equilateral triangle on the base. We assume that the centre of equilateral triangle is the origin of the coordinate system OXYZ, the Z axis is in the gravity direction, and the X axis in the direction perpendicular to the connection line of *Isolator 1* and *Isolator 3*. As is shown in Fig. 2, the displacement between each two isolators is L, and the three isolators distribute on the circle with the radius equates R.

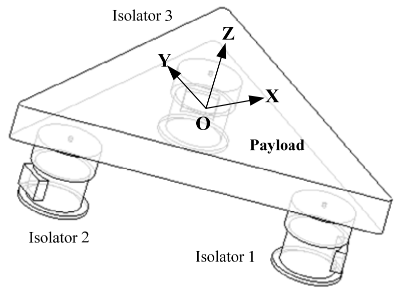

Fig. 1 Layout of AVIS

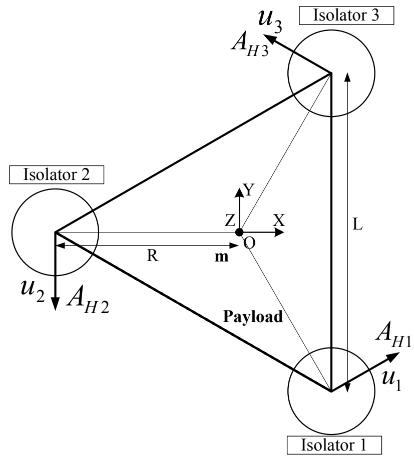

Fig. 2 Geometry of AVIS φ_x

The system geometry is depicted in Fig. 2. It shows both the sensor and actuator locations together with the centre of gravity, indicated with m, with respect to the virtual reference point indicated with O. In the coordinates system OXYZ, the Cartesian coordinates of the system is defined as

$$\boldsymbol{\theta} = \begin{bmatrix} x & y & \varphi_z & z & \varphi_x & \varphi_y \end{bmatrix}^T$$

Six geophone sensors and six eddy sensors are used to measure the absolute velocity and the relative position of the payload. So the measurement results is written as

$$A = \begin{bmatrix} A_{H1} & A_{H2} & A_{H3} & A_{V1} & A_{V2} & A_{V3} \end{bmatrix}^T$$

where V indicates the vertical direction and H indicates the horizontal direction, A_{Hi} and A_{Vi} ($i = 1, 2, 3$) denotes the horizontal and vertical velocity (or displacement) signals for i-th isolator.

Because the angles φ_x , φ_y , and φ_z are very small [1], the sensor output in terms of generalized position or velocity is given by

$$\boldsymbol{\theta} = \boldsymbol{T_S A}$$

$$\boldsymbol{T_S} = \begin{bmatrix} \sqrt{3}/2 & 1/2 & R & 0 & 0 & 0 \\ 0 & -1 & R & 0 & 0 & 0 \\ \sqrt{3}/2 & 1/2 & R & 0 & 0 & 0 \\ 0 & 0 & 0 & 1 & -1/2R & -1/2L \\ 0 & 0 & 0 & 1 & R & 0 \\ 0 & 0 & 0 & 1 & -1/2R & 1/2L \end{bmatrix}^{-1}$$

where matrix $\boldsymbol{T_S}$ is used to transform the measurement results of geophones and eddy sensors from physical axis into logical axis.

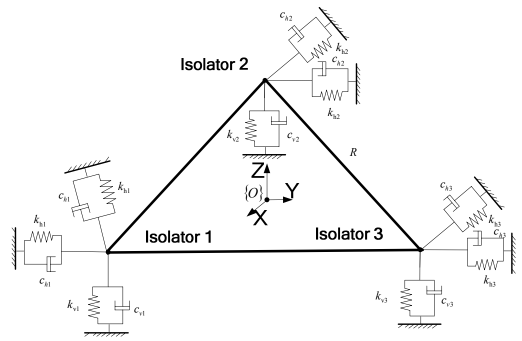

Fig. 3 Model of structure dynamics

Based on the principle of structure dynamics, each vibration isolator is equivalent to three mutually orthogonal springs and dampers, as shown in Fig. 3 [1, 14]. By using the Euler-Lagrange formalism, the load dynamic equation is expressed as

$$\boldsymbol{M}\ddot{\boldsymbol{\theta}} + \boldsymbol{C}\dot{\boldsymbol{\theta}} + \boldsymbol{K}\boldsymbol{\theta} = \boldsymbol{F_M} \tag{1}$$

where $\boldsymbol{M}$ represents a symmetric mass matrix

$$\boldsymbol{M} = \begin{bmatrix} m & & & & & \\ & m & & & & \\ & & I_z & & & \\ & & & m & & \\ & & & & I_x & \\ & & & & & I_y \end{bmatrix}$$

$\boldsymbol{C}$ is a symmetric damping matrix

$$\boldsymbol{C} = \begin{bmatrix} c_{11} & c_{12} & c_{13} & 0 & 0 & 0 \\ c_{21} & c_{22} & c_{23} & 0 & 0 & 0 \\ c_{31} & c_{32} & c_{33} & 0 & 0 & 0 \\ 0 & 0 & 0 & c_{44} & c_{45} & c_{46} \\ 0 & 0 & 0 & c_{54} & c_{55} & c_{56} \\ 0 & 0 & 0 & c_{64} & c_{65} & c_{66} \end{bmatrix}$$

$$c_{11} = c_{22} = c_{h1} + c_{h2} + c_{h3}, c_{12} = c_{21} = 0,$$
$$c_{13} = c_{31} = \frac{\sqrt{3}}{2} R c_{h1} - \frac{\sqrt{3}}{2} R c_{h3},$$
$$c_{23} = c_{32} = \frac{1}{2} R c_{h1} - R c_{h2} + \frac{1}{2} R c_{h3},$$
$$c_{33} = R^2 c_{h1} + R^2 c_{h2} + R^2 c_{h3}, c_{44} = c_{v1} + c_{v2} + c_{v3},$$
$$c_{45} = c_{54} = -\frac{\sqrt{3}}{2} R c_{v1} + \frac{\sqrt{3}}{2} R c_{v3},$$
$$c_{46} = c_{64} = -\frac{1}{2} R c_{v1} + R c_{v2} - \frac{1}{2} R c_{v3},$$
$$c_{55} = \frac{3}{4} R^2 c_{v1} + \frac{3}{4} R^2 c_{v3},$$
$$c_{56} = c_{65} = \frac{\sqrt{3}}{4} R^2 c_{v1} - \frac{\sqrt{3}}{4} R^2 c_{v3},$$
$$c_{66} = \frac{1}{4} R^2 c_{v1} + R^2 c_{v2} + \frac{1}{4} R^2 c_{v3}.$$

$\boldsymbol{K}$ is a symmetric stiffness matrix

$$\boldsymbol{K} = \begin{bmatrix} k_{11} & k_{12} & k_{13} & 0 & 0 & 0 \\ k_{21} & k_{22} & k_{23} & 0 & 0 & 0 \\ k_{31} & k_{32} & k_{33} & 0 & 0 & 0 \\ 0 & 0 & 0 & k_{44} & k_{45} & k_{46} \\ 0 & 0 & 0 & k_{54} & k_{55} & k_{56} \\ 0 & 0 & 0 & k_{64} & k_{65} & k_{66} \end{bmatrix}$$

$$k_{11} = k_{22} = k_{h1} + k_{h2} + k_{h3}, k_{12} = k_{21} = 0,$$
$$k_{13} = k_{31} = \frac{\sqrt{3}}{2} R k_{h1} - \frac{\sqrt{3}}{2} R k_{h3},$$
$$k_{23} = k_{32} = \frac{1}{2} R k_{h1} - R k_{h2} + \frac{1}{2} R k_{h3},$$
$$k_{33} = R^2 k_{h1} + R^2 k_{h2} + R^2 k_{h3}, k_{44} = k_{v1} + k_{v2} + k_{v3},$$
$$k_{45} = k_{54} = -\frac{\sqrt{3}}{2} R k_{v1} + \frac{\sqrt{3}}{2} R k_{v3},$$
$$k_{46} = k_{64} = -\frac{1}{2} R k_{v1} + R k_{v2} - \frac{1}{2} R k_{v3},$$
$$k_{55} = \frac{3}{4} R^2 k_{v1} + \frac{3}{4} R^2 k_{v3},$$
$$k_{56} = k_{65} = \frac{\sqrt{3}}{4} R^2 k_{v1} - \frac{\sqrt{3}}{4} R^2 k_{v3}$$
$$k_{66} = \frac{1}{4} R^2 k_{v1} + R^2 k_{v2} + \frac{1}{4} R^2 k_{v3}$$

and $\boldsymbol{F_M}$ is the matrix of the control force in logical axis $\boldsymbol{\theta}$

$$\boldsymbol{F_M} = \begin{bmatrix} F_x & F_y & F_{rz} & F_z & F_{rx} & F_{ry} \end{bmatrix}^T$$

The actuator output $\boldsymbol{F_L}$ in terms of physical coordinates is given by

$$\boldsymbol{F_L} = \boldsymbol{T_S}^{-1} \boldsymbol{F_M}$$

2.2. Control strategies

As shown in Fig. 4, Six single input, single output (SISO) controllers with a velocity feedback and a position feedback are used to compensate the vibrations in six directions. The decoupling matrix $\boldsymbol{T_S}$ is calculated from geometric relations. Sensor matrix $\boldsymbol{T_S}$ is used to transform the measurement results of geophones and eddy sensors from physical axis into logical axis. Actuator decoupling matrix $\boldsymbol{T_A}$ is used to transform the control signal from logical axis into actuator axis. With the coupling matrix and decoupling matrix, the 6×6 multiple input, multiple output (MIMO) controllers of AVIS are reduced to six SISO controllers in six logical axes. A velocity proportional-integral-derivative (PID) controller is used to increase the damping, and a position PID controller to maintain the position stability.

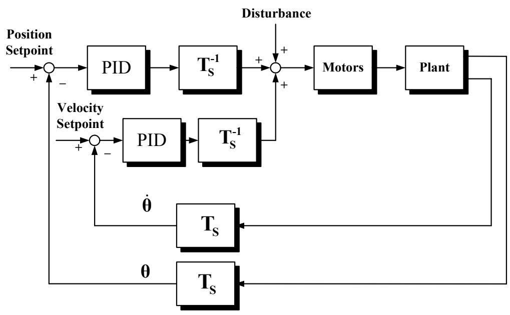

Fig. 4 Control block of the AVIS

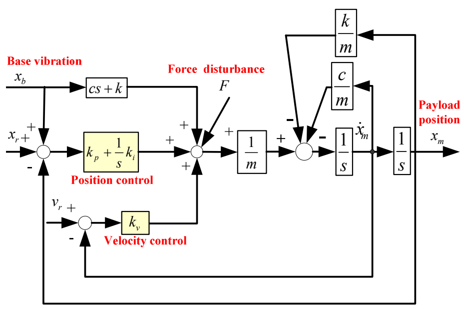

Fig. 5 Control schematic of SISO controller

As the structure coupling is weak in six orthogonal coordinates, six SISO feedback controllers can be self-tuned separately. For each logical axis, the control schematic of SISO feedback is simplified as shown in the Fig. 5. Only 3 parameters of a typical SISO controller, velocity proportional gain k_v, position proportional gain k_p and integral gain k_i, must be determined with self-tuning procedures. Besides these 3 parameters, SISO controller includes notch filters and lowpass filters. The notch filters, which are used to depress the structure modes, depend on the actual systems and their parameters are easily determined. The lowpass filters are used to depress high frequency noise, and the cross frequency for velocity loop is commonly set to 50 Hz while the cross frequency for the position loop is about 10 Hz. To simplify the question, the self-tuning controller only determines the 3-PID parameters.

3. Self-tuning method for SISO feedback

The payload vibration is caused by both base vibration and direct force disturbance. As shown in Fig. 4, the transfer function $H_{x_b}^{x_m}(s)$ from base x_b to payload x_m and transfer function $H_F^{x_m}(s)$ from direct disturbance force F to payload x_m can be deprived and normalized as

$$H_{x_b}^{x_m}(s)=\frac{cs^2+(k+k_p)s+k_i}{ms^3+(c+k_v)s^2+(k+k_p)s+k_i} \tag{2}$$

$$H_F^{x_m}(s)=\frac{X_m(s)}{F(s)}=\frac{1}{ms^2+(c+k_v)s+k+k_p+\frac{1}{s}k_i} \tag{3}$$

Normalizing Eq. 2 and Eq. 3 with respect to ω_n, s_n, ξ_1, ξ, m and η, we can get

$$H_{x_b}^{x_m}(s)=\frac{2\xi_1 s_n{}^2+s_n+\eta}{s_n{}^3+2\xi s_n{}^2+s_n+\eta} \tag{4}$$

$$H_F^{x_m}(s)=\frac{1}{\omega_n{}^2 m}\frac{s_n}{s_n{}^3+2\xi s_n{}^2+s_n+\eta} \tag{5}$$

with

$$\left.\begin{aligned}&\frac{1}{m}(k+k_p)=\omega_n{}^2,\frac{1}{m}(c+k_v)=2\xi\omega_n\\&\frac{c}{m}=2\xi_1\omega_n,\frac{k_i}{m}=\eta\omega_n{}^3,s_n=\frac{s}{\omega_n}\end{aligned}\right\} \tag{6}$$

It should be noted that the parameters k_p, k_i and k_v do not appear in Eq. 4 and Eq. 5, and the mechanical parameters ω_n and m only appear as gains. These imply that only the parameter ξ_1 is needed to determine the optimum control parameters for the feedback control parameters ξ and η. The parameter ξ_1 must be very small to achieve high vibration isolation performance in high-frequency band. Its typical value is set to 0.02. As the parameters ξ and η are determined, the parameter ω_n can be optimized by minimizing the vibration of the payload.

So we can follow the following procedure: first determine the damping rate ξ and integration rate η, and then determine the ω_n.

3.1. Damping rate ξ and integration rate η

a) Stability

Fig. 6 is root locus with different integration rate η. The damping rate ξ and integration rate η are limited into the stable area shown in Fig. 7.

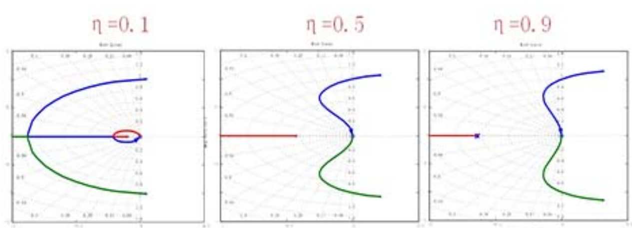

Fig. 6 Root locus with different integration rate η

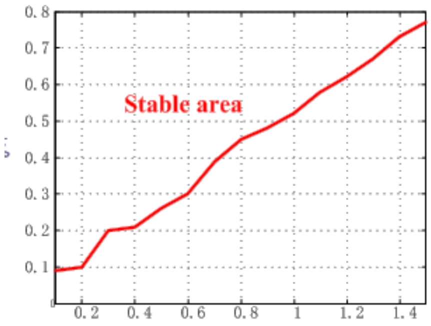

Fig. 7 Stable area

b) Base vibration isolation

Fig. 8 denotes the vibration transmissibility from base at resonance frequency according to the integration rate η and the damping rate ξ. In order to limit the vibration transmissibility resonance into 5 dB, η and ξ are limited into the area of "Resonance < 5 dB" as shown in Fig. 8.

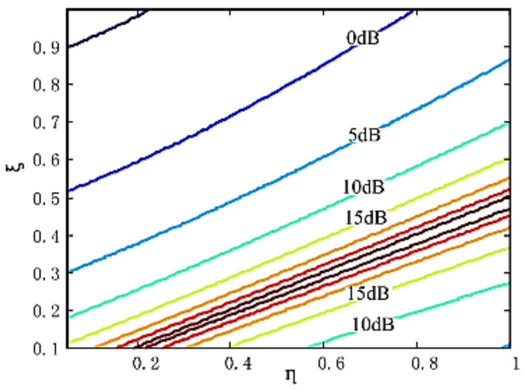

Fig. 8 Resonance vibration transmissibility contour

c) Setting-time

With step disturbance on the payload, the setting-time is restricted by the η and ξ at the same ω_n.

The position response to step disturbance force on the payload is shown in Fig. 9, where P_0 and T_0 are the position response amplitude and period without active control separately.

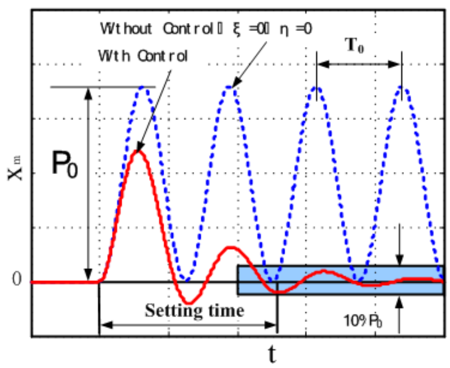

Fig. 9 Step response of $H_F^{x_m}(s)$

To limit the setting time into T_0, η and ξ are restricted into the area of 'Setting time $1T_0$' area, as shown in Fig. 10.

Above all, the optimal η and ξ should set into $1T_0$ range. Damping $\xi = 0.7$ and $\eta = 0.36$ are recommend to achieve maximum damping rate.

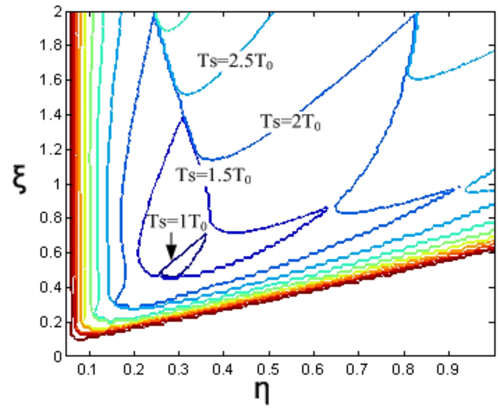

Fig. 10 Settling time contour according to η and ξ

3.2. Resonance frequency ω_n

The resonance frequency affects the vibration level of the payload. By minimization of accumulate acceleration PSD (Power Spectral Density) on the payload, the resonance frequency ω_n is achieved. The accumulate acceleration PSD on the payload is defined as follows

$$\left.\begin{array}{l} J = \displaystyle\int_{\omega=\omega_1}^{\omega=\omega_2} \left(S_F(\omega) \left| H_F^{a_m}(j\omega) \right|^2 + S_B(\omega) \left| H_{a_b}^{a_m}(j\omega) \right|^2 \right) d\omega \\ \omega_n \geq \omega_{n1} \end{array}\right\} \quad (7)$$

where $H_F^{a_m}(j\omega)$ is the acceleration response of disturbance force F, $H_{a_b}^{a_m}(j\omega)$ is the vibration transmissibility from base, $S_B(\omega)$ is the base vibration PSD, and $S_F(\omega)$ is the disturbance force PSD.

By minimization of J in Eq. 7, the optimal resonance frequency ω_n can be calculated.

4. Simulation on self-tuning controller

4.1. Self-tuning procedure for AVIS:

a) calculation of the sensor decoupling matrix and actuator decoupling matrix, based on the geometry relations;

b) estimation of system parameters in six logical axes, such as relative damping c, stiffness k, mass m.

This parameter estimation approaches are divided into indirect and direct techniques who work together to use online [2, 15, 16].

c) Determination of the optimal controller parameters.

Follow the procedure of chapter 3, we can calculate the feedback control parameters.

$$\begin{cases} k_p = m\omega_n^2 - k \\ k_v = 1.4m\omega_n - c \\ k_i = 0.36m\omega_n^3 \end{cases} \quad (8)$$

4.2. Calculation

We take a metrology frame as a example. The payload mass is 1300 kg, and the moments of inertia are: $I_{xx} = 184.6$ kgm^2, $I_{yy} = 193.7$ kgm^2, $I_{zz} = 373.9$ kgm^2. From the following parameters: $R = 0.65$ m, $k_{h1} = k_{h2} = k_{h3} = 6.7e^4$ N/m, $k_{v1} = k_{v2} = k_{v3} = 8.2e^4$ N/m, $c_{h1} = c_{h2} = c_{h3} = 500$ N/m, and $c_{v1} = c_{v2} = c_{v3} = 600$ Ns/m, the damping matrix $\boldsymbol{C}$ and Stiffness matrix $\boldsymbol{K}$ are determined.

There are two primary vibrations, vibration from base floor and direct disturbance acoustics, the acceleration PSD of base vibration is depicted in Fig. 11 while the random disturbance force caused by acoustics noise below the level of 0.01 N.

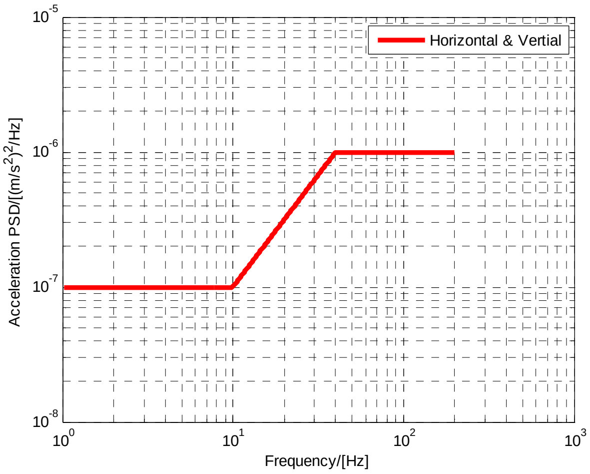

Fig. 11 Base acceleration PSD level

The resonance frequencies ω_n for each SISO loop are optimized based on the Eq. 7. All three parameters are then calculated based on the Eq. 8. The results are depicted in the Table.

Table

Controller parameters

Axis	k_p	k_v	k_i
X	$1e^{-4}$	$1.7e^5$	$3.2e^5$
Y	$1e^{-4}$	$1.7e^5$	$3.2e^5$
Rz	$1e^{-4}$	$6e^3$	$1.6e^5$
Z	$1e^{-4}$	$2.5e^4$	$8.9e^5$
Rx	$1e^{-4}$	$4.2e^3$	$2.3e^5$
Ry	$1e^{-4}$	$4.3e^3$	$2.2e^5$

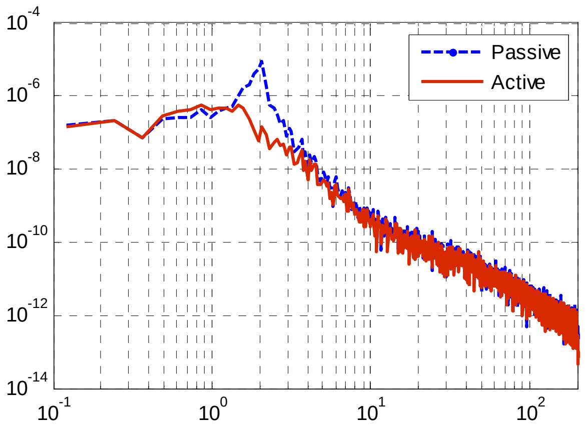

Fig. 12 Horizontal acceleration PSD comparison with the use of self-tuning controller

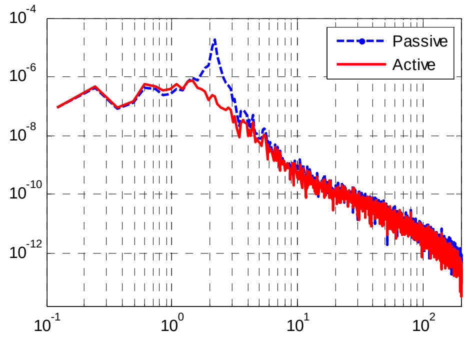

Fig. 13 Vertical acceleration PSD comparison with the self-tuning controller

The metrology vibration with or without using self-tuning controller are shown in Figs. 12 and 13. With active control, the resonant PSD is dropped down to below 10^{-6} (m/s^2)^2/Hz, and the horizontal acceleration and vertical acceleration are depressed to 10^{-8} (m/s^2)^2/Hz in the frequency range above 3 Hz and above 4 Hz separately.

5. Experiment and verification

To verify the vibration isolation performance of self-tuning controller, an experiment is executed. The AVIS test platform is shown in Fig. 14. The payload is supported by three vibration isolators, and all the parameters are described in Chapter 4. The vibration source includes base vibration disturbance and acoustics noise disturbance. The vibration level is measured using the self-tuning controller.

Lightweight piezoelectric accelerometers (PCB 352A10 ICP accelerometers, frequency range 0.003 -10 kHz, sensitivity ~ 1.052 mV/m/s^2, 0.7 gr) are used to measure the base vibration and metrology frame vibration at two locations at the same direction. The measured signals are conditioned and subsequently sampled by a SigLab data acquisition module (featuring four 20-bit simultaneously sampled A/D channels, two 16-bit D/A channels, and analog 4-th order quasielliptic anti-aliasing filter).

Compared with the base vibration, the effects of acoustics noise can be ignored. The self-tuning controller of AVIS is turned on with the parameters listed in Table. Both the base and payload vibration are measured by accelerometers, which are shown in Figs. 15 and 16.

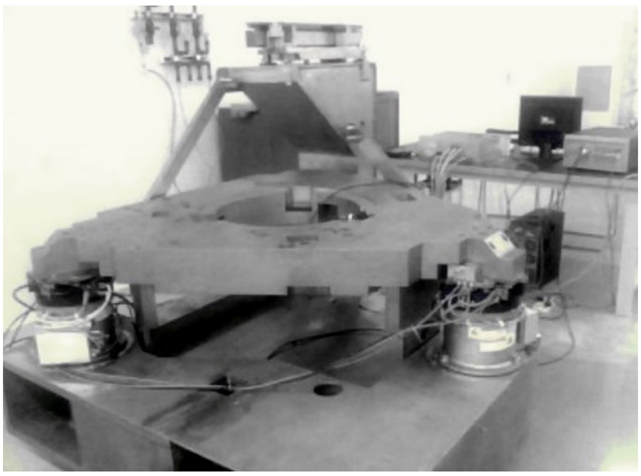

Fig. 14 Platform of AVIS

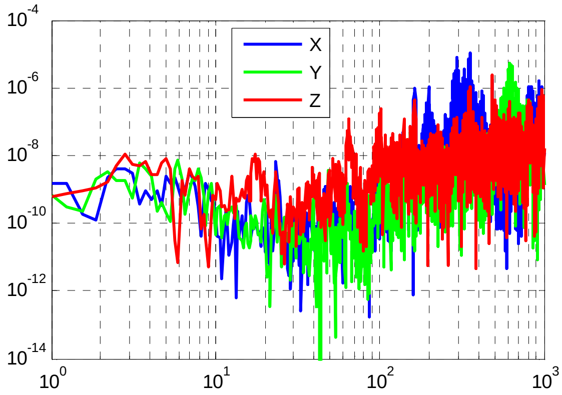

Fig. 15 Base acceleration PSD

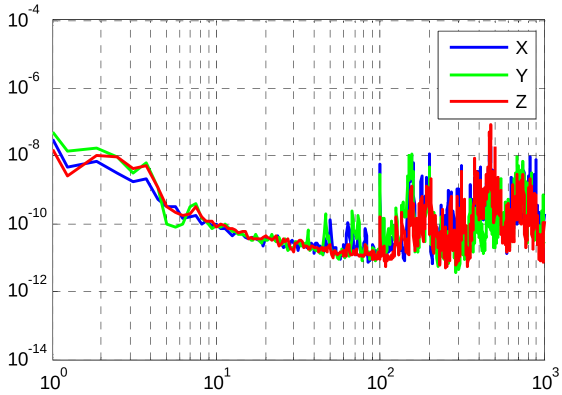

Fig 16 Payload acceleration PSD with active control

Fig. 16 shows that the PSD level of payload acceleration is satisfied and Fig. 16 shows that the acceleration PSD value is below the level of 10^{-10} $(m/s^2)^2/Hz$ in the frequency range of 10 Hz to 100 Hz. These imply that the self-tuning controller can achieve high vibration isolation performance and shorten the tuning time.

6. Conclusion

A self-tuning procedure is proposed for 6-DOF AVIS with position feedback and velocity feedback, which aims at optimal damping of AVIS with Sky-hook. As the structure coupling is weak in six orthogonal coordinates, self-tuning is realized in three steps: calculation of the decoupling matrix, identification of the structure parameters based on the dynamic model of the AVIS, optimization of the feedback controller by minimizing the vibration of the payload. An experiment is implemented to verify the self-tuning method and the performance of AVIS with a metrology test platform. The acceleration PSD value is below the level of 10^{-10} $(m/s^2)^2/Hz$ in range of 10 Hz and 100 Hz by using the self-tuning controller. Compared with the traditional loop shaping method, this self-tuning procedure can quickly and efficient determine the feedback control parameters and doesn't depend on operator's experience.

References

1. **Heertjes, M.; Graaff, K.; Toorn, J.G.** 2005. Active vibration isolation of metrology frames; a modal decoupled control design, Journal of Vibration and Acoustics 127: 223-233.

2. **Kato, H.; Wakui, S.; Mayama, T.; et al.** 1999. System identification of anti-vibration units in semiconductor exposure apparatus, Proc. IEEE. International Conference on Control Applications, Kohala Coast-Island of Hawai'I, USA.

3. **Yoshioka, H.; Takahashi, Y.; et al.** 2001. An active microvibration isolation system for Hi-tech manufacturing facilities, Journal of Vibration and Acoustics 123: 269-275.

4. **Jakštas, A.; Kaušinis, S.; Flügge, J.** 2005. Investigation of calibration facilities of precision line scales, Mechanika 3(53): 62-67.

5. **Ibrahim, R.A.** 2008. Recent advances in nonlinear passive vibration isolatiors, Journal of Sound and Vibration 314: 371-452.

6. **Kimmenade, J.; et al.** 1994. Positioning device with a force actuator system for compensating center-of-gravity displacements, and lithographic device provided with such a positioning device, US Patent, 5844664.

7. **Loopstra, E.R.; Heiland, P.** 2001. Supporting device provided with a gas spring with a gas bearing, and lithographic device provided with such supporting devices, US Patent, 6226075.

8. **Beard, A.M; Schuber, D.W, and von Flotow, A.H.** 1994. A practical product implementation of an active/passive vibration isolation system, Active Control of Vibration and Noise, ASME DE-Vol, 75: 485-492.

9. **Kato, T.; Kawashima, K.; Sawamoto, K.; et al.** 2007. Active control of a pneumatic isolation table using model following control and a pressure differentiator, Precision Engineering 31: 269-275.

10. **Kawashima, K.; Kato, T.; Swamoto, K.; et al.** 2007. Realization of virtual sub chamber on active controlled pneumatic isolation table with pressure differentiator, Precision Engineering 21: 139-145.

11. **Preumont, A.; Francois, A.; et al.** 2002. Force feedback versus acceleration feedback in active vibration isolation, Journal of Sound and Vibration 257(4): 605-613.

12. **Karnopp, D.C.; Trikha, A.K.** 1969. Comparative study of optimization techniques for shock and vibration isolation, Trans, ASME. J. of Engineering for Industry, Series B, 91: 1128-1132.

13. **Karnopp D.** 1995. Active and semi-active vibration isolation, ASME Journal of Mechanical Design, 117: 177-185.

14. **Rademakers, N.G.M.** 2005. Modelling, identification and multivariable control of an active vibration isolation system, Master's thesis, Eindhoven University of Technology.

15. **Brad, B.M.; Hurlebaus, S.; Stöbener, U.; et al.** 2005. Modeling and parameter identification of an active anti-vibration system, Proc. SPIE 5760: 23-34.

16. **Holterman, J. and Vries, T.** 2000. Self-tuning integral force feedback, Proc. 5th International Conference on Motion and Vibration Control 'MOVIC 2000', Sydney, Australia, 643-648.

F. H. Liao, X. P. Li, Z.Y. Yuan

ŠEŠIŲ LAISVĖS LAIPSNIŲ AKTYVIOS SVYRAVIMŲ IZOLIACIJOS SISTEMOS PADĖTIES IR GREIČIO RYŠIO SUSIREGULIAVIMAS

R e z i u m ė

Aktyvios vibroizoliacijos sistema (AVIS), sukomponuota su pozicijos ir greičio grįžtamojo ryšio jutikliais, plačiai naudojama IC įrenginiuose ir didelio tikslumo metrologijos prietaisuose aukštoms svyravimo izoliacijos charakteristikoms ir padėties stabilumui užtikrinti. Tačiau aktyvios vibroizoliacinės sistemos (AVIS) charakteristikos visada yra veikiamos padėties ir greičio grįžtamojo ryšio fazinių priklausomybių. Tradiciškai greičio ir grįžtamojo ryšio parametrų kontrolė yra nustatoma derinant šiuos parametrus. Tačiau šioms derinimo problemoms spręsti reikia daug laiko, o AVIS, valdoma šiais parametrais, nepasiekia geresnių charakteristikų. Šiame straipsnyje siūlomas AVIS susireguliavimo procesas naudojant greičio ir padėties grįžtamuosius ryšius, kurie optimaliai slopina AVIS. Kai konstrukciniai ryšiai yra silpni, šešiose ortogonaliosiose koordinatėse susireguliavimo procedūra yra atliekama trimis žingsniais: nesujungtos matricos skaičiavimu; AVIS dinaminio modelio konstrukcinių parametrų identifikavimu; grįžtamojo ryšio valdiklio optimizavimu, minimizuojant svyravimus. Susireguliavimo metodui ir AVIS charakteristikoms patikrinti atliktas eksperimentas.

F. H. Liao, X. P. Li, Z. Y. Yuan

SELF-TUNING OF POSITION FEEDBACK AND VELOCITY FEEDBACK OF ACTIVE VIBRATION ISOLATION SYSTEM WITH 6 DOFS

S u m m a r y

Active Vibration Isolation Systems (AVIS), which are composed of position feedback loop and velocity feedback loop, are widely used in IC equipments and high precision metrology devices to achieve high vibration isolation performance and maintain position stability. However, the performance of AVIS is always affected by both position feedback loop and velocity feedback loop. Traditionally, the control parameters of the velocity loop and feedback loop are determined in sequence. But theses tuning procedures are time-consuming and the performance of AVIS greatly depends on operator's experience. Further more, AVIS controlled with these parameters can not attain the best performance. In this paper, we propose a self-tuning procedure for the AVIS with velocity feedback and position feedback, which aims at optimal damping of AVIS with Sky-hook. As the structure coupling is weak in six orthogonal coordinates, the self-tuning procedure is realized in three steps: calculation of the decoupling matrix, identification of the structure parameters based on the dynamic model of the AVIS, optimization of the feedback controller by minimizing the vibration of payload. A simulation and an experiment are implemented to verify the self-tuning method and the performance of AVIS.

Received March 28, 2011
Accepted November 05, 2011